RSC Advances

PAPER

View Article Online
View Journal | View Issue

Cite this: *RSC Adv.*, 2021, **11**, 10681

Highly robust, novel aluminum counter cation-based monophosphate tungsten bronze electro-catalysts for oxygen evolution in acidic solution†

Md. Imran Hossain,[a] Tapas Debnath,[b] M. Yousuf Ali Mollah,[a] Md. Abu Bin Hasan Susan[a] and Md. Mominul Islam*[a]

This study describes the successful synthesis of novel bronze with a low tungsten oxidation state for the efficient electro-catalytic oxidation of water. An extraordinarily robust monophosphate tungsten bronze (MPTB)-modified graphite anode was successfully fabricated for the oxygen evolution reaction (OER) at a thermodynamic potential of 1.23 V in H_2SO_4 acidic solution. Several Al, Cr and Fe counter-cation-based MPTBs were synthesized by the solution combustion method. Novel Al-based MPTBs calcined at 700 °C in O_2 (AlO7) showed almost zero onset overpotential, high current density, high turnover frequency for OER and steady catalysis in repeated use even after 30 weeks. The orthorhombic AlO7 comprising crystallites of 9.89 nm and an indirect band gap (1.89 eV), is an unusually stable MPTB that contains 98% W^{5+} state stabilized with the Al^{3+} counter cation. The catalysis decreases as the ratio of W^{5+} : W^{6+} in MPTBs decreases and [410] and [601] facets play main roles in the first H_2O association and nucleophilic attack of the second H_2O molecule on the catalyst surface. Thus, MPTBs can be non-noble metal anode materials for robust acidic H_2O electrolyzers.

Received 26th January 2021
Accepted 25th February 2021

DOI: 10.1039/d1ra00699a

rsc.li/rsc-advances

1. Introduction

The modern world demands clean and renewable forms of energy to overcome the current environmental crisis.[1] The generation of energy from renewable sources and the development of efficient storage and safe distribution protocols are the most attractive domains for current research. Energy sectors consistently pursue innovative batteries, capacitors, supercapacitors, *etc.*, to store electrical energy and these systems require huge storage chemicals that are limited, create secondary waste, pollute the environment and are toxic to living beings. In the $H_2O \leftrightarrow H_2$ cycle, H_2 gas is a high density clean energy carrier. The $H_2O \leftrightarrow H_2$ cycle has been considered an energy storage alternative to batteries and capacitors. Moreover, H_2 gas fuel is used in the H_2–O_2 fuel cell, but the green production of H_2 gas from different sources, including H_2O, is still costly, which actually prolongs the flourishing of fuel cell technology and keeps it primitive.

The formation of O_2 and H_2 gases from H_2O involves:

$$2H_2O(l) \rightarrow O_2(g) + 4H^+(aq) + 4e^- \text{ at anode} \quad (1)$$

$$2H^+(aq) + 2e^- \rightarrow H_2(g) \text{ at cathode} \quad (2)$$

The thermodynamic potential of overall water splitting is 1.23 V *versus* the normal hydrogen electrode (NHE). In practice, an excess potential called overpotential (η) has to be applied to regulate cell reactions. The overall potential (η_{op}) for water splitting can be described as[2]

$$\eta_{op} = 1.23 + \eta_a + |\eta_c| + \eta_\Omega \quad (3)$$

where η_a and η_c are overpotentials required to surmount the intrinsic activation barriers of the anode and cathode, respectively, and η_Ω represents the excess potential required to overcome internal resistance, including solution and contact resistance. An extremely large η_a is usually needed to achieve the oxygen evolution reaction (OER) (eqn (1)).[3] Dau *et al.* and Man *et al.* have reported that OER, due to its sluggish kinetics, is the impediment for overall H_2O splitting.[4,5] The slow kinetics of OER is caused by the complexity associated with $4e^-/4H^+$ removal (eqn (1)) and the thermodynamically difficult formation of the new O–O bond in O_2.[6–9] OER involves several intermediate steps involving different oxygen containing intermediates, namely peroxide, superoxide and hydroxyl radicals (Scheme 1).[10]

The effective activation of molecules that can minimize these intrinsic barriers takes place through their binding, with suitable conformations, to the active sites of a heterogeneous catalyst, from which the intermediate species should not be

[a]*Department of Chemistry, Faculty of Science, University of Dhaka, Dhaka 1000, Bangladesh. E-mail: mominul@du.ac.bd*

[b]*Department of Theoretical and Computational Chemistry, Faculty of Science, University of Dhaka, Dhaka, Bangladesh*

† Electronic supplementary information (ESI) available. See DOI: 10.1039/d1ra00699a

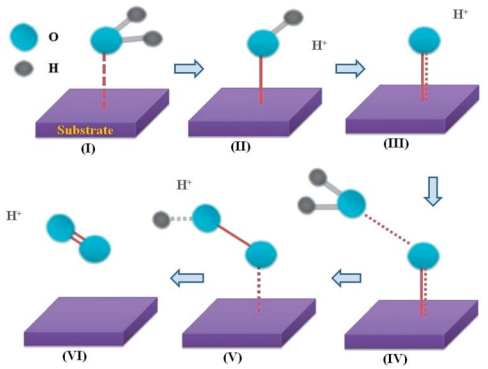

Scheme 1 General mechanism for OER at catalytic surface. Different stages of OER at the electrode surface: (I) water association, (II) first proton-coupled electron transfer (PCET), (III) second PCET, (IV) nucleophilic attack, (V) third PCET and (VI) fourth PCET and evolution of O_2.

desorbed until the product is formed. To improve the activity of electro-catalysts, two general strategies have been applied: (i) active site engineering and (ii) conductivity optimization. The former is based on the particle size, morphology, intrinsic and lattice defects, and crystallinity that maximize the density of accessible active sites.[11] The second is improved by doping with hetero-atoms which may minimize the intrinsic activation energy (charge-transfer resistance) and η_a in a composite type catalyst.[11,12] Substantial efforts have been devoted to designing efficient OER catalysts other than precious metal-based ones, *e.g.*, Pt, RuO_2, and IrO_2, which are known to show superior catalytic activities but have no real possibility to scale up to meet global demand due to their scarcity.[13,14] The η_a of OER studied on a FeO_x adsorbed indium-tin oxide electrode in phosphate buffer was found to be 580 mV.[15] Iron dopants have been found to play a critical role in enhancing the activity of Ni-based electrocatalyts.[16] Nano-sized layered aluminum or zinc-manganese oxides have been found to show efficient OER activity in the presence of cerium(IV) ammonium nitrate as a non-oxo transfer oxidant, wherein aluminum or zinc ions have been shown to play a key role in the catalysis.[17] The redox-active center of $Ru_4(\gamma\text{-}SiW_{10})_2$ immobilized on multi-walled carbon nanotubes decorated with poly(amidoamine) ammonium dendrimers showed greatly improved catalysis in OER and performed multiple functions: (i) the co-existence of tungsten (W) and ruthenium (Ru) sites enhanced the hydrophilic character of the catalyst, creating a suitable environment for H_2O adsorption, (ii) the charged nitrogen and oxygen residues assisted H_2O diffusion into the molecular cavity and (iii) the coordination and hydrogen bonding interactions stabilized OER intermediates until product formation.[18] Blasco *et al.* reported that the enhanced catalytic activity of polyoxometalates (POMs) with cesium or barium counter-cations for OER occurred at an η_a of 189 mV *vs.* NHE in acidic solution.[19] These catalysts suffer from a stability problem in acidic solution. The earth abundant and inexpensive catalysts perform well in alkaline or neutral media[2] in which $|\eta_c|$ is high to regulate the H_2 evolution (eqn (2)) that eventually increases the η_{op} (eqn (3)).

Here we report, for the first time, the synthesis and use of extraordinarily stable monophosphate tungsten bronze (MPTB) catalysts that perform OER in acidic media at the thermodynamic potential. MPTBs are polyanion clusters with structural diversity in which the oxometal polyhedra of MO_x (in the present case, WO_x and $x = 5, 6$), are the basic units and the polyanions act as Lewis acid or base under different conditions.[18] The MPTB family was chosen because of their low dimensionality[20] and their polyanions make it easy to selectively incorporate the desired counter-cations close to their active sites to regulate and stabilize the oxidation state (*i.e.*, x = either 5 or 6) of the central metal (*e.g.*, W). In this study, three series of MPTBs based on Al, Cr and Fe counter cations were prepared through solution combustion synthesis (SCS) and were calcined at different temperatures in either O_2 or N_2 atmosphere. Approximately zero onset η_a, high current density at low η_a, high turnover frequency (TOF) and robust electro-catalytic stability in repeated performances of OER in H_2SO_4 solution were achieved with the Al-based MPTB deposited on a graphite electrode. The reason for the persistent catalytic activity of the studied MPTBs was revealed by analyzing the catalysts with state-of-the-art techniques.

2. Experimental

2.1. Materials

The analytical grade chemicals and materials, such as potassium chloride (KCl, Sigma, Germany), potassium bromide (KBr, Sigma-Aldrich, Germany), sulphuric acid (H_2SO_4, Merck, Germany), ethanol (C_2H_5OH, Merck, Germany), poly(vinylidene fluoride) (PVdF, Sigma-Aldrich, Germany), tungstic acid (H_2WO_4, Sigma, Japan), ammonium dihydrogen phosphate ($NH_4H_2PO_4$, Sigma, Japan), chromium(III) nitrate nonahydrate ($Cr(NO_3)_3 \cdot 9H_2O$, Merck, Germany), iron(III) nitrate nonahydrate ($Fe(NO_3)_3 \cdot 9H_2O$, Merck, Germany), aluminum nitrate nonahydrate ($Al(NO_3)_3 \cdot 9H_2O$, Merck, Germany) as a source of trivalent cations, glycerin (Sigma-Aldrich, Germany), and graphite rods (Alfa Aesar, USA), were used without further purification. Distilled water was passed through HPLC grade water purification systems (BOECO, BOE 8082060, Germany) to yield de-ionized water (conductivity: 0.055 $\mu S\ cm^{-1}$ at 25.0 °C) for use throughout the experiments.

2.2. Syntheses of catalysts

MPTBs were prepared by the SCS method, which involves uniform preheating of the reaction mixture prior to self-ignition.[21,22] Appropriate amounts of tungstic acid (H_2WO_4) and metal (Al, Cr and Fe) nitrates were dissolved in a minimum amount of aqueous ammonia. Glycerin and ammonium dihydrogen phosphate, which acted as a fuel and oxidizer, respectively, were added in a ratio of 1 : 8 in all runs.[22,23] The colored, solid mass was treated in a tube furnace (ESI†) and the conditions of synthesis and abbreviated names of the catalysts can be seen in the captions of figures and in Table S1.†

2.3. Deposition of prepared catalysts on electrode surface

The prepared MPTBs were deposited on a graphite disk electrode (diameter *ca.* 0.615 cm). Each mixture of a particular

MPTB and PVdF binder was prepared with the appropriate amount of these compounds (Table S7†). Typically, MPTB and *ca.* 15% binder were dispersed in ethanol. These mixtures were sonicated in an ultrasonic bath for 15 min and the dispersed solid mass was deposited on a flat, polished graphite electrode by the solution casting method in which the dispersion was added dropwise to the surface of electrode. The ethanol evaporated within 5 min. A thin layer of MPTB, as indicated by the characteristic color, was obtained by heat treatment at 100 °C in an oven. The thickness of the fabricated MPTB on the graphite electrode was determined by spectrometer (Model: AvaSpec-ULS2048-USB2, Avantes, Netherlands) where white light interference and the pattern were translated into optical thickness. The reference spectrum was taken from a clean bare graphite electrode and a spectrum of a fabricated graphite electrode was obtained. The average thickness of these thin films was around 160 nm as found from the difference of these two spectra.

2.4. Electrochemical measurements

A single compartment three-electrode cell was used for the electrochemical measurements in which the data were recorded using a computer-controlled electrochemical analyzer system (Model: CHI 760E, USA). The electrochemical measurements were conducted in 0.08 M H_2SO_4 electrolytic solution using a modified graphite electrode as the working electrode, a spiral Pt wire electrode as the counter electrode and a silver|silver chloride|saturated KCl solution [Ag|AgCl|KCl (sat.)] as the reference electrode. Linear sweep voltammograms (LSVs) measured at various experimental conditions were analyzed to evaluate the catalytic performance of MPTBs for OER in 0.08 M H_2SO_4 solution. The η_a was determined as the potential corresponding to the intersection point of the tangent lines drawn from the rising current and baseline current of an LSV. The applied potential was converted to η_a in the NHE scale[19] by the mathematical manipulations described in the ESI.† The dependence of j on η_a can be depicted by Tafel plots. The overpotential is generally logarithmically related to j and its linear portion is given as the Tafel equation (eqn (4)) where (η > 0.05 V)[2,42]

$$\eta = a + b \log j \quad (4)$$

where b is the Tafel slope and is related to the mechanism of the electrode reaction.

The value of TOF was determined from the experimental j and charge (Q) according to[2]

$$\mathrm{TOF} = j_\eta/(4 \times Q) \quad (5)$$

where j_η is the current density at the applied potential η and 4 is number of electrons involved with the OER. The TOF number of a catalyst characterizes its level of activity. In fact, TOF is the total number of moles transformed into the desired product by one mole of active site per second. To calculate TOF, j_η and Q were determined from LSV (Fig. 3b) and chronocoulometric data (Fig. S11†).

3. Results and discussion

3.1. Material characterizations

MPTBs were subjected to systematic, comprehensive analyses as described. The typical SEM images (Fig. 1) present the characteristic stony surface of AlO7 and AlN7 particles; the particles of AlO7 are larger in size than those of AlN7. Detailed morphological analyses of the synthesized MPTBs are given in the ESI (Table S2†). Particle counts for scales of both 10 and 100 nm are higher for AlN7 than AlO7. The Fe-based MPTB showed its characteristic spongy surface (Fig. S3†). To reveal the composition and chemical state of W and other elements in MPTBs, FTIR and XPS analyses were carried out for AlO7 and AlN7 (Fig. 2).

Intense bands at 600–659 cm^{-1} for the characteristic stretching vibration of W–O–W and a broad band at 1100 cm^{-1} for the stretching vibration of Al–O were observed in the FTIR spectrum of AlO7 (Fig. S1†).[24] Similarly, the characteristic bands for the stretching vibrations of Cr–O and Fe–O in the FTIR spectra of Cr- and Fe-based MPTBs were noted (see ESI†). Only Al-based MPTBs were purposely subjected to further characterization. Fig. 2a represents the typical de-convoluted XPS spectrum of tungsten 4f in AlO7. Asymmetric doublets assignable to 34.03 and 36.10 eV for W^{5+} of $4f_{7/2}$ and $4f_{5/2}$, respectively, were observed, along with a weak peak at 37.52 eV for $4f_{5/2}$ of the W^{6+} oxidation state (Fig. 2a).[25] Characteristic peaks at 133.5 and *ca.* 530.0 eV for phosphorus 2p in phosphate and 1s of lattice oxygen, respectively, confirm the formation of MPTB (Fig. S7†).[26,27] UV-visible reflectance spectra of AlO7 and AlN7 are shown in Fig. S4.† One prominent absorption band is observed in the region of 200 to 500 nm. These spectral analyses also support the presence of W with different oxidation states in which W^{5+} is significantly greater (*ca.* 98%) than W^{6+} (*ca.* 2%) in AlO7. In contrast, the amount of W^{5+} in AlN7 decreased to *ca.* 60% (Fig. S4 and Table S4†). The Al^{3+} counter-cation in MPTB donates its electrons to the vacant t_{2g} orbital and stabilizes W^{5+} states.[28,29] The W^{5+} state of bronze continuously converts to stable W^{6+} in an open environment, leading to a characteristic color change. It is noteworthy that no such color change of MPTBs, especially for the Al-series, was observed, indicating that we succeeded for the first time in synthesizing MPTBs with a stable W^{5+} state with the assistance of Al^{3+} counter cations that actually play the key role in the catalysis of OER, *vide infra*.

The derivation of absorption spectrum fitting (DASF) method[30] was applied to gain more insight into the band gap

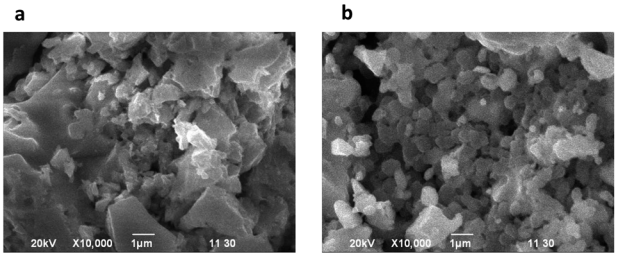

Fig. 1 (a and b), SEM images of AlO7 and AlN7, respectively.

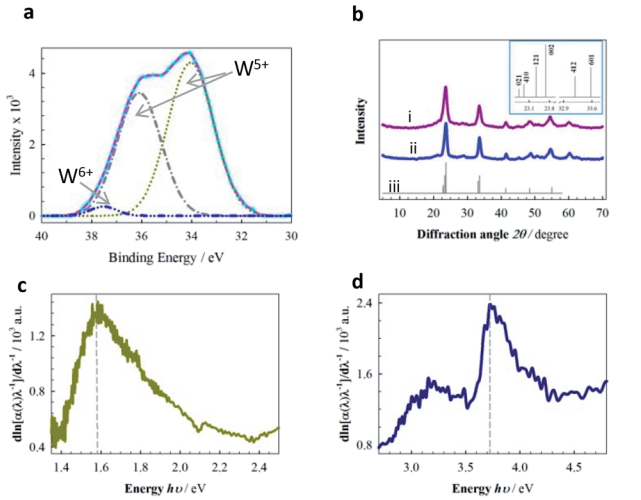

Fig. 2 (a) XPS spectra of W 4f for AlO7. (b) XRD patterns of (i) AlN7, (ii) AlO7 and (iii) calculated refined response. Inset represents lower 2θ zone of calculated XRD response with the Miller indices. (c and d) Derivative response obtained from the experimental reflectance data of AlO7 and AlN7, respectively, using the DASF method.[30] AlO7 and AlN7 refer to Al-based MPTBs calcined at 700 °C in O_2 and N_2 atmospheres, respectively.

energy (E_g) and the nature of the transition in AlO7 and AlN7. The Kubelka–Munk method[31] was initially applied to determine the absorption coefficient. The systematic calculation of E_g is described in Table S3 and Fig. S5, S6. † The transition is indirect, meaning there is a misalignment of crystal momentum between the minimum energy level of the conduction band and the maximum energy level of the valence band. However, the E_g of AlO7 (1.58 eV) is less than one-half that of AlN7 (3.72 eV) (Fig. 2c and d).

This can be supported by considering the presence of a high percentage of the Al^{3+} state in AlO7 (Fig. S7b†), which lowers the E_g and hence increases conductivity, as identified by electrochemical impedance spectroscopy (Fig. S12†). The band gap of AlN7 at an E_g of 3.16 eV is due to the increase in quantum confinement due to the agglomeration of particles.[32]

The XRD diffraction lines shown in Fig. 2b indicate that AlO7 and AlN7 are crystalline in nature and the crystal system of these MPTBs is orthorhombic (ESI†).[33] WO_3 is normally cubic polymorph, which is thermodynamically unstable.[34] In 1989, Siedle *et al.* [34] speculated that if WO_3 could be specially doped with Al, the degree of inversion of Al^{3+} in octahedral sites would take place at the available O^{2-} lattices[30] and hence enhance the stability of the W^{5+} state (Fig. 2a). The calculated Miller indices of AlO7 are higher and the high-index facets, such as [410] and [601], are the surfaces of the lattice (Table S6†) where the atoms are located further apart. These atoms are ready to bond to more potential neighbors if the crystal continues to grow and this leads to a higher surface free energy than in the low-index facets, showing high catalytic activity.[35,36] The crystallite sizes of AlO7 were determined to be larger (9.89 nm) than those of AlN7 (7.45 nm), supporting the SEM observations (ESI†).

3.2. Electrocatalytic performance of MPTBs

The catalytic performances of three series of MPTBs deposited on graphite electrodes for OER were tested in 0.08 M H_2SO_4 solution. Fig. 3a presents the cyclic voltammograms (CVs) recorded; no significant peak could be distinguished except for the anodic shoulder at 1.185 V *vs.* NHE for OER. LSVs of OER recorded with three representative MPTBs are compared in Fig. 3b. Similar LSVs for OER were also measured for all compounds under consideration. From the measured LSV responses, the η_{onset}, Tafel slope and TOF were evaluated and are summarized in Fig. 4.

At a glance, AlO7 shows the lowest η_{onset} of 4 mV for OER among the other MPTBs studied. Importantly, this η_{onset} is almost zero, that is, the OER started at its thermodynamic potential. A similar observation for AlN7 can also be seen. The η_{onset} generally increases with Al-series MPTB samples calcined at temperatures lower or higher than 700 °C. In addition, η_{onset} was found to slightly increase to 45 mV after continuous performance of OER for 18 h. The corresponding Tafel slope and TOF for AlO7 were determined to be 370 mV dec^{-1} and 0.049 s^{-1}, respectively.

The role of Al in MPTBs for this catalysis in OER was further investigated by replacing Al^{3+} with Cr^{3+} and Fe^{3+}. As can be seen in Table S8† and Fig. 3 and 4, the η_{onset} values with CrO7, CrO8, FeO7 and FeO8 are higher than those of the corresponding series of Al-based MPTBs. In this case, the Tafel slopes are also much higher than those obtained with Al-based MPTBs. Moreover, the TOFs are significantly low. Therefore, Al-based MPTBs are superior in all respects to the other two series of MPTBs studied. Other important characteristics of an OER catalyst are the η_a corresponding to the current density (j) of 10 mA cm^{-2} (η_{10}), which is the maximum efficiency of a solar cell reported so far,[37,38] and the stability. The η_{10} for AlO7 was 620 mV *vs.* NHE (Fig. 5a). In addition, the chronoamperometric j–t response (Fig. 5b) clearly evidenced that AlO7 is highly stable, with about a 2-times higher limiting j than those obtained with CrO7 and FeO8. Blasco-Ahicart *et al.* investigated

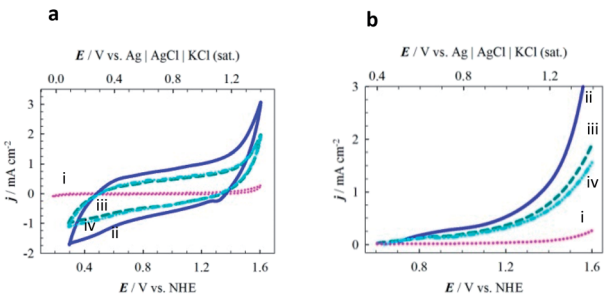

Fig. 3 Comparative electrochemical behavior of MPTB-modified graphite electrodes in acidic media. (a) CVs and (b) background-corrected LSVs of OER measured with (i) bare, (ii) AlO7-, (iii) CrO7- and (iv) FeO8-modified graphite electrodes in 0.08 M H_2SO_4 solution at a potential scan rate of 5 mV s^{-1}. In AlO7, CrO7 and FeO8 MPTB catalysts, Al, Cr and Fe refer to the counter-cations of Al^{3+}, Cr^{3+} and Fe^{3+}, the digits 7 and 8 refer to the calcination temperatures of 700 and 800 °C, respectively, and O stands for a calcination atmosphere of O_2.

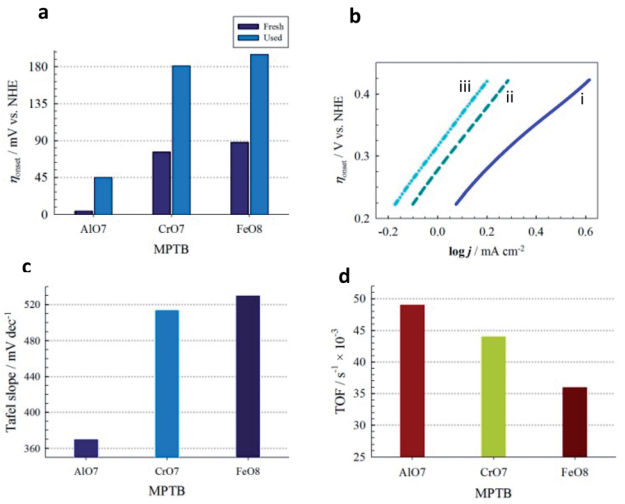

Fig. 4 (a) Comparison of η_{onset} determined with freshly fabricated and tested (for continuous OER at a constant potential of 1.51 V *vs.* NHE for 18 h) electrodes. (b) Tafel plot: (i) AlO7, (ii) CrO7 and (iii) FeO8. (c) Tafel slope. (d) TOF of OER.

OER in 1.0 M H_2SO_4 solution with cobalt oxides and cobalt-based POMs with counter-cations of cesium and barium (Ba[Co-POM]) and compared the results of catalytic performance with state-of-the-art IrO_2 catalyst.[19] IrO_2 exhibited an η_{onset} of *ca.* 340 mV and η_{10} of *ca.* 500 mV. The lowest η_{onset} of *ca.* 90 mV and η_{10} of *ca.* 360 mV with a Tafel slope of 97 mV dec^{-1} were observed with Ba[Co-POM] incorporated in a carbon paste electrode.[19] They reported a decreasing trend in j for the OER measured at an η_a of 250 mV for 24 h. In contrast, the stability of OER studied at an η_a of 324 mV exhibited that the AlO7 catalyst is highly stable and, interestingly, the current increases with time. Almost no change in the OER response was noticed after keeping the AlO7 modified electrode in the measured solution for 30 weeks. This suggests that the prepared MPTB is highly stable in an open environment.

Three main concerns, namely the origin of the low η_{onset}, the extraordinary stability of MPTBs and the pathway of OER, are addressed here. The solution resistance and charge-transfer resistance were found to be negligibly small, at 17.2 and 37.8 Ω, respectively. In addition, the electro-conductivity of AlO7 which can be manifested by a low E_g (Table S3†) should be high. Such an enhanced electrical conductivity of AlO7 would likely be facilitated through the formation of a two-dimensional (2D) layer-type structure. A relatively low content of PO_4^{3-} in AlO7 (Fig. S8†) is suitable for the stability of the observed orthorhombic phase and suggests the formation of a 2D layered structure (Fig. S9†).[28] In addition, the observation of a large number of oxygen vacancies in AlO7 and a low E_g also supports the high conductivity of AlO7.[39] All of these combined together minimize the η_{onset} of OER at AlO7 to almost zero. The reason for the increasing trend of j with time, shown in Fig. 5b, is ambiguous, but may be associated with the enhancement of catalytic activity *via* the spin-exchange phenomenon.[40] The MPTBs studied, especially the Al-based series, are paramagnetic in nature,[41] possessing an unpaired electron that may assist the inversion of the singlet state of O_2, formed as an intermediate during OER, to a stable triple state of O_2 (stage V, Scheme 1). This spin inversion occurs simultaneously by flipping the spin of the electron in the e_g orbital of the W^{5+} ion in AlO7 to be parallel,[40] which is considered to enhance the catalytic activity.

The catalytic current is proportional to the reaction rate over the electrode surface that is potential dependent[42] and the catalytic OER consists of number of elementary steps (Scheme 1). The activity and reaction mechanism of the electrocatalyst can be revealed by examining the sensitivity of the current against applied potential (Fig. 4c) and their slopes (Tafel slope), as compared in Fig. 4c. A low Tafel slope suggests the surface-adsorbed species produced in the early stage of OER remains predominant, while a high Tafel slope indicates the occurrence of competition between a chemical and an electron-transfer limiting step during OER.[19] In Fig. 6, a hypothetical pathway for the MPTB-catalyzed OER is proposed. The adsorption of H_2O would occur on the active metal (W^{5+}) sites with a higher oxidation state.[43] Thus, the e_g orbital of the W^{5+} ion of AlO7 participates in σ-bonding with a surface H_2O molecule[44,45] to enhance H_2O association (stage I, Scheme 1).

The coordinated tungsten hydroxide starts to form through the first PCET reaction. The second PCET occurs to form {W–O–H} and another molecule of H_2O takes part in a third PCET process to form {W–O–O–H}. In the following fourth PCET mechanism, O_2 gas is evolved and these steps continue in a cyclic

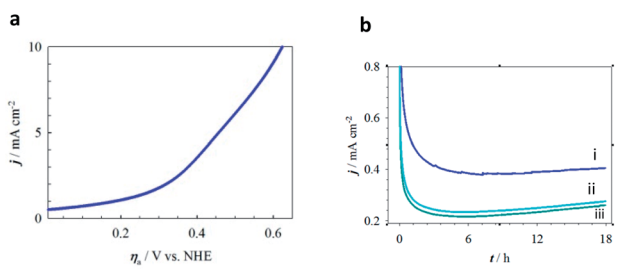

Fig. 5 Electrocatalytic stability for OER at MPTB-modified graphite electrodes in acidic media. (a) LSV of AlO7 in 0.08 M H_2SO_4 solution at a scan rate of 5 mV s^{-1}. (b) Chronoamperometric data for (i) AlO7, (ii) CrO7 and (iii) FeO8 at a constant potential of η_a = 324 mV *vs.* NHE.

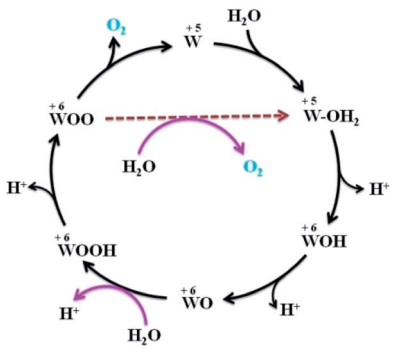

Fig. 6 Probable electrochemical OER mechanism at MPTB in acidic media.[46]

manner. Since the rate-determining step faces the highest kinetics hurdle, to attain a high j, *i.e.*, to achieve an acceptable rate of OER, a higher potential must be applied. Formation of WOOH is the slowest step (*i.e.*, the rate-determining step) because the thermodynamic energy barrier for surface oxygen coupling (stage IV, Scheme 1) is possibly larger than that of the associative reaction (stage I, Scheme 1).[47] The Al-based MPTBs definitely enhance H_2O association (stage I), but their direct role in surface oxygen coupling involving nucleophilic attack is also a burgeoning question that may be clarified by quantum mechanical calculations and computer modeling.

4. Conclusions

Highly stable Al^{3+} counter-cation-supported W^{5+} state-enriched MPTB and Cr^{3+} and Fe^{3+} counter-cation-based MPTBs were prepared by SCS method and characterized by FTIR, SEM imaging, XPS, reflectance and XRD techniques. The band gaps of the Al-based MPTB are indirect in nature and the values of E_g decrease by changing the calcination atmosphere from N_2 to O_2 due to the formation of the 2D-layered structure of the orthorhombic phase of AlO7. The catalytic performances of all MPTBs towards electrochemical OER varied widely as established by comparing η_{onset}, Tafel slope and TOF and were revealed to be associated with the ratios of the W^{5+} : W^{6+} states in the MPTBs, which entirely depend on the counter-cations[48] and calcination[49] conditions. The robustness of AlO7 in catalysis is rationally achieved due to the unusual stability of W^{5+} in MPTB created by the incorporation of Al^{3+}, as explained earlier.[34] The e_g orbital of W^{5+}, particularly of the high-index facets of [410] and [601], in AlO7 may participate in σ-bonding with a surface H_2O molecule[44,45] to enhance the H_2O association step and the nucleophilic attack of a second H_2O molecule on the catalyst surface. Such self-coordination of H_2O to the surface of the catalyst reasonably reduces the associated kinetic hurdles, offering OER at a low η_a. Thus, the developed anode is promising for the design of a cost-effective, efficient electrolyzer for large scale production of H_2 fuel from H_2O.

Conflicts of interest

There are no conflicts to declare.

Acknowledgements

Authors are grateful to Dr Altaf Hussain, retired professor of the Department of Chemistry, University of Dhaka (DU) and currently working as an academic advisor in Bangabandhu Sheikh Mujibur Rahman Maritime University, Bangladesh for his supports in designing and synthesizing bronze compounds. Authors thank Dr S. M. A. Hakim Siddiki, Institute of Catalysis, Hokkaido University, Japan for supporting the XPS analysis. Authors are also grateful to Dr Mangir Murshed, Solid State Chemical Spectroscopy Division, University of Bremen, Germany for discussing about DASF method used for calculation of band gap energy and Dr Subrata Roy, Department of Chemistry, Jagannath University, Bangladesh for sharing his expertise in XRD analysis of tungsten-bronze compounds. The instrumental supports of CARS, DU used for characterizing MPTB samples are also greatly acknowledged. MMI acknowledges the financial support as a special allocation for research of the Ministry of Science and Technology, Bangladesh. MIH acknowledges the financial supports in the form of fellowships of the University Grants Commission, Bangladesh and the Bose Centre for Advanced Study and Research in Natural Sciences, DU.

References

1 J. H. Bentley, *Procedia Social and Behavioral Sciences*, 2013, 77, 108–115.
2 M. M. Islam and M. S. Miran, in *Innovations in Engineered Porous Materials for Energy Generation and Storage Applications*, ed. R. Rajagopalan and A. Balakrishnan, CRC Press, Boca Raton, 2018, pp. 267–288.
3 C. C. L. McCrory, S. Jung, I. M. Ferrer, S. M. Chatman, J. C. Peters and T. F. Jaramillo, *J. Am. Chem. Soc.*, 2015, **137**, 4347–4357.
4 I. C. Man, H. Y. Su, F. Calle-Vallejo, H. A. Hansen, J. I. Martínez, N. G. Inoglu, J. Kitchin, T. F. Jaramillo, J. K. Nørskov and J. Rossmeisl, *ChemCatChem*, 2011, **3**, 1159–1165.
5 H. Dau, C. Limberg, T. Reier, M. Risch, S. Roggan and P. Strasser, *ChemCatChem*, 2010, **2**, 724–761.
6 L. G. Bloor, P. I. Molina, M. D. Symes and L. Cronin, *J. Am. Chem. Soc.*, 2014, **136**, 3304–3311.
7 B. C. M. Martindale and E. Reisner, *Adv. Energy Mater.*, 2016, **6**, 1–9.
8 S. Trasatti, *J. Electroanal. Chem.*, 1972, **39**, 163–184.
9 S. Trasatti, *Electrochim. Acta*, 1984, **29**, 1503–1512.
10 J. M. Gonçalves, T. A. Matias, K. C. F. Toledo and K. Araki, *Adv. Inorg. Chem.*, 2019, **74**, 241–303.
11 D. Yan, Y. Li, J. Huo, R. Chen, L. Dai and S. Wang, *Adv. Mater.*, 2017, **29**, 1606459.
12 L. Han, S. Dong and E. Wang, *Adv. Mater.*, 2016, **28**, 9266–9291.
13 L. Duan, F. Bozoglian, S. Mandal, B. Stewart, T. Privalov, A. Llobet and L. Sun, *Nat. Chem.*, 2012, **4**, 418–423.
14 R. D. L. Smith, B. Sporinova, R. D. Fagan, S. Trudel and C. P. Berlinguette, *Chem. Mater.*, 2014, **26**, 1654–1659.
15 E. Pizzolato, S. Scaramuzza, F. Carraro, A. Sartori, S. Agnoli, V. Amendola, M. Bonchio and A. Sartorel, *J. Energy Chem.*, 2016, **25**, 246–250.
16 L. Trotochaud, S. L. Young, J. K. Ranney and S. W. Boettcher, *J. Am. Chem. Soc.*, 2014, **136**, 6744–6753.
17 M. M. Najafpour, B. Pashaei and S. Nayeri, *Dalton Trans.*, 2012, **41**, 7134–7140.
18 S. S. Wang and G. Y. Yang, *Chem. Rev.*, 2015, **115**, 4893–4962.
19 M. Blasco-Ahicart, J. Soriano-Lopez, J. J. Carbo, J. M. Poblet and J. R. Galan-Mascaros, *Nat. Chem.*, 2018, **10**, 24–30.
20 P. Roussel, O. Pérez and P. Labbé, *Acta Crystallogr., Sect. B: Struct. Sci.*, 2001, **57**, 603–632.
21 A. Kopp Alves, C. P. Bergmann and F. A. Berutti, *Novel Synthesis and Characterization of Nanostructured Materials*, Springer, Berlin, 2013, p. 11.

22 A. S. Mukasyan, P. Epstein and P. Dinka, *Proc. Combust. Inst.*, 2007, **31**, 1789–1795.
23 T. Mimani and K. C. Patil, *Mater. Phys. Mech.*, 2001, **4**, 134–137.
24 R. Romero Toledo, V. Ruiz Santoyo, C. D. Moncada Sánchez and M. Martínes Rosales, *Nova Scientia*, 2018, **10**, 83.
25 Y. Liu, S. Shrestha and W. E. Mustain, *ACS Catal.*, 2012, **2**, 456–463.
26 S. Lee, M. Choi and J. Kim, *IEEE Trans. Magn.*, 2017, **53**, 1–5.
27 S. Du, C. Zhang, P. Jiang and Y. Leng, *ACS Appl. Nano Mater.*, 2019, **2**, 7432–7440.
28 M. Greenblatt, *Int. J. Mod. Phys. B*, 1993, **7**, 3937–3971.
29 W. Grünert, E. S. Shpiro, R. Feldhaus, K. Anders, G. V. Antoshin and K. M. Minachev, *J. Catal.*, 1987, **107**, 522–534.
30 L. I. Granone, A. C. Ulpe, L. Robben, S. Klimke, M. Jahns, F. Renz, T. M. Gesing, T. Bredow, R. Dillert and D. W. Bahnemann, *Phys. Chem. Chem. Phys.*, 2018, **20**, 28267–28278.
31 D. P. Joseph and C. Venkateswaran, *J. At., Mol., Opt. Phys.*, 2011, **2011**, 1–7.
32 T. Edvinsson and R. Soc, *R. Soc. Open Sci.*, 2018, **5**, 1–17.
33 D. A. Woodcock, P. Lightfoot and C. Ritter, *J. Solid State Chem.*, 2000, **149**, 92–98.
34 A. R. Siedle, M. L. Brostrom, T. E. Wood, D. C. Koskenmaki, B. Montez and E. Oldfield, *J. Am. Chem. Soc.*, 1989, **111**, 1665–1669.
35 Y. Sun, S. Zhang, W. H. Zhang and Z. Y. Li, *Chin. J. Chem. Phys.*, 2018, **31**, 485–491.
36 L. L. Feng, G. Yu, Y. Wu, G. D. Li, H. Li, Y. Sun, T. Asefa, W. Chen and X. Zou, *J. Am. Chem. Soc.*, 2015, **137**, 14023–14026.
37 J. D. Benck, T. R. Hellstern, J. Kibsgaard, P. Chakthranont and T. F. Jaramillo, *ACS Catal.*, 2014, **4**, 3957–3971.
38 Q. Gao, W. Zhang, Z. Shi, L. Yang and Y. Tang, *Adv. Mater.*, 2019, **31**, 1–35.
39 E. Fabbri and T. J. Schmidt, *ACS Catal.*, 2018, **8**, 9765–9774.
40 F. A. Garcés-Pineda, M. Blasco-Ahicart, D. Nieto-Castro, N. López and J. R. Galán-Mascarós, *Nat. Energy*, 2019, **4**, 519–525.
41 R. R. Rakhimov and A. I. Aleksandrov, *J. Phys. Chem. B*, 2000, **104**, 10973–10977.
42 T. Shinagawa, A. T. Garcia-Esparza and K. Takanabe, *Sci. Rep.*, 2015, **5**, 1–21.
43 J. Carrasco, A. Hodgson and A. Michaelides, *Nat. Mater.*, 2012, **11**, 667–674.
44 S. Yagi, I. Yamada, H. Tsukasaki, A. Seno, M. Murakami, H. Fujii, H. Chen, N. Umezawa, H. Abe, N. Nishiyama, *et al.*, *Nat. Commun.*, 2015, **6**, 1–6.
45 J. Suntivich, K. J. May, H. A. Gasteiger, J. B. Goodenough and Y. Shao-Horn, *Science*, 2011, **334**, 1383–1385.
46 M. Schilling and S. Luber, in *Advances in Inorganic Chemistry*, ed. R. V. Eldik and C. D. Hubbard, Academic Press, Cambridge, 2019, vol. 74, pp. 61–114.
47 J. K. Nørskov, T. Bligaard, A. Logadottir, S. Bahn, L. B. Hansen, M. Bollinger, H. Bengaard, B. Hammer, Z. Sljivancanin, M. Mavrikakis, *et al.*, *J. Catal.*, 2002, **209**, 275–278.
48 S. C. Roy, W. Assenmacher, T. Linden, L. Esser, W. Mader and R. Glaum, *Zeitschrift für Naturforschung B*, 2016, **71**, 543–552.
49 G. Leftheriotis, S. Papaefthimiou, P. Yianoulis and A. Siokou, *Thin Solid Films*, 2001, **384**, 298–306.